The platination mechanism of RNase A by arsenoplatin: insight from the theoretical study†

A. Parise, [a,b] N. Russo [a] and T. Marino *[a]

Herein, we present a detailed metalation process of the bovine pancreatic ribonuclease (RNase A) by a novel multitarget anti-cancer agent arsenoplatin-1, **AP1**, ([Pt(μ-NHC(CH_3)O)$_2$ClAs(OH)$_2$]), on the basis of quantum chemical investigation, employing the B3LYP and M062x functionals and a large model of the active site. The proposed mechanism is consistent with the structural data. The role of water molecules in the active site is also analyzed. These studies revealed that the Nδ of His119 binds platinum(II), preserving the Pt–As bond. To better rationalize the different behavior of **AP1** (bound to His119) and the reference cisplatin (bound to Met29) towards the same target RNAse A, also these processes have been considered. The final platinated complex structure agrees well with the crystallographic one. Our results evidence that the metalation process takes place more favorably in water than in the protein environment in agreement with the nature of the protein binding pocket residues.

Introduction

The O'Halloran group successfully developed a synthesis method to obtain good amounts of stable aqueous arsenous acid–platinum complex with biological activity that is distinct from cisplatin and arsenic trioxide individually. This newly synthesized compound, named arsenoplatin-1 (**AP1**), [Pt(μ-NHC(CH_3)O)$_2$ClAs(OH)$_2$] (Scheme 1), presented anticancer biological activity in several cancer cell lines and is stable in an aqueous environment. In addition, it can be beneficial to load it into a liposome based drug delivery system. With the aim of improving the efficacy of these two common anti-cancer therapeutics, a method to co-encapsulate high levels of arsenous acids and aqua-cisPt into 100 nm liposomes, capable of releasing their drug in the low-pH endosome, has been developed.[1]

Arsenoplatins are a good example of hybrid bifunctional compounds obtained from merging the pharmacophores of active molecules featuring different mechanisms of action. They are adducts of two chemically important anticancer drugs, cisplatin and arsenic trioxide, characterized by an arsenous acid moiety covalently linked to the platinum(II) center equipped with an unusual five coordinate As(III)-geometry. This can be interpreted, in the drug discovery field, as a borderline choice between bio-inspired and rational design generating molecules with a dual mode of action for creating new efficient drugs that can act on different biological targets. Preliminary tests *in vitro* aimed to evaluate the cytotoxicity proposed that arsenoplatins may have a distinct mode of action in comparison with cisplatin and As_2O_3 alone, other than the ability to overcome platinum resistance mechanisms.[2]

Arsenoplatin-1 (**AP1**) resulted to be more potent than either cisplatin or arsenic trioxide in most of the cancer cell lines evaluated. This behavior was deemed attributable to a possible cooperative effect between platinum and arsenic pharmacophores detected in lungs,[3] oral squamous cell carcinoma,[4] and ovarian cancer cell lines.[5]

Despite the insights gained into the interaction of cisplatin and **AP1** with DNA at theoretical and experimental levels,[2,6] those concerning **AP1** and proteins are often lacking. Recently, with the aim of better learning its biological chemistry, a novel investigative strategy based on the combined use of electrospray ionization mass spectrometry (ESI MS) and X-ray crystallography[7,8] allowed the in-depth investigation of the

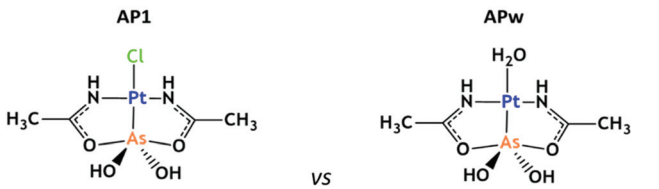

Scheme 1 Representation of the **AP1** complex and its aquated form **APw**.

metalation process of small model proteins. In particular, the structural information of the hen egg white lysozyme (HEWL) and bovine pancreatic ribonuclease (RNase A), interacting with cisplatin, is available.[9] Recent structural studies have shown that **AP1** bound to RNase A with platinum(II) that binds to the N-atoms of the solvent exposed His105 and His119 side chains on the surface of the protein preserving the Pt–As bond.[10] Since His119 residues are implicated in the catalytic activity of the RNase A enzyme, the binding of **AP1** on this site results in the inhibition of the enzyme function, as indicated by a catalytic activity assay. Unlike **AP1**, cisplatin showed the adduct formation with the methionine sulfur atom under the same conditions. In addition, analogous to what was observed with the tested proteins, the same authors observed **AP1** readily enters the cells and binds to DNA, maintaining the Pt–As bond (Pt : As ratio of 1). After longer incubation times, however, the Pt : As ratio in DNA samples increases, suggesting the occurrence of cleavage of the Pt–As bond and the release of the As $(OH)_2$ moiety. This finding suggested that arsenoplatin-1 has the potential to deliver both Pt and As species to a variety of hematological and solid cancers with superior effects to those observed in most parts of the NCI-60 human tumor cell lines when compared to the use of cisplatin or arsenic trioxide as single agents.

Starting from these interesting experimental outcomes[2,10] and stimulated by the reliable results of the previous theoretical investigation on the **AP1**–DNA interaction mechanisms,[6] it seemed right, but also intriguing, to explore the inhibition mechanism induced by the metalation process of RNase A at the expense of **AP1**. To do this, a rather large quantum chemical model including amino acid residues present in the catalytic task and suitable to describe electronic structures and related energetic profiles has been adopted. Furthermore, to find an explanation of the different behavior of **AP1** (bound to His119) and cisplatin (bound to Met29) towards the same target RNase A, the mechanism has been explored by using smaller models.

Theoretical calculations represent nowadays an effective way to separate and individually quantify the physical components that contribute to the activation free energy and, therefore, are an optimal tool to characterize all the species including intermediates and transition states, intercepted along a selected reaction pathway, often suggested by the experimental findings.

Computational methods

All the calculations were performed employing the Gaussian 09.D01 software package.[11] The B3LYP[12,13] (20% HF exchange) and M062x[14] (54% HF exchange) functionals coupled to the 6-31+G(d,p) basis set for the C, N, O, and H atoms were used for the small models (Scheme S1†). The results for geometry optimization, electronic barrier height and electronic energy of reaction are reported in Fig. S1.† On the basis of these results, for larger systems, the M062x functional was employed. Furthermore, to evaluate the influence of the exchange–correlation functional also single point B3LYP computations on the M06-2x optimized geometries were performed.

For both Pt and As atoms, the effective core potential SDD[15] coupled with their related orbital basis set was selected. The D3 dispersion contribution was considered in all the computations.[16]

In order to avoid large artificial movements of the amino acids in the larger quantum cluster model, the coordinate-locking scheme was assumed in which the amino acid residues are usually truncated at Cα atoms that are fixed during geometry optimizations. The stars in Fig. 1 indicate the atoms where the truncation is made. The residues have been modelled according to standard cluster model procedures.[17–24] This adopted procedure assumes that the overall structure is kept very close to the experimental one. The nature of minima (no negative vibrational frequencies) and transition states (one negative vibrational frequency) along potential energy surfaces was established by frequency calculation at the same level of theory. Due to the presence of constrained atoms, small vibrational frequencies <40i cm^{-1} have been obtained in all stationary points that do not alter the thermochemical analysis and zero-point energy (ZPE) corrections and do not obscure the main negative TS-frequency. An analogous computational protocol was successfully applied in the mechanistic studies of many enzymes.[23–29]

The transition state has been checked by intrinsic reaction coordinate (IRC) analysis,[30,31] by assessing that the localized transition states correctly connect to the corresponding minima along the imaginary mode of vibration.

To model the protein environment effects, the CPCM[32,33] polarizable continuum model was used with a dielectric con-

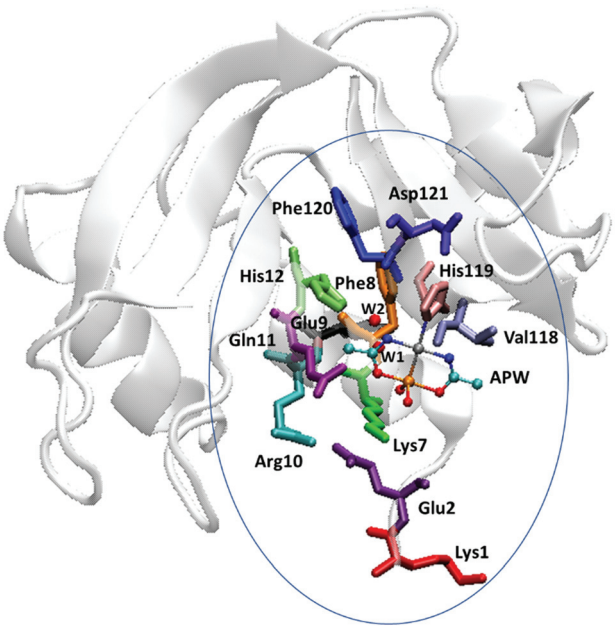

Fig. 1 The used cluster model is shown inside the circle and the arsenoplatin complex is shown as balls and sticks.

stant that simulates the protein (ε = 4) and water (ε = 80) environments. The last choice well reproduces the nature of the catalytic pocket that is widely solvent exposed.[10] To improve the electronic energies, the more extended 6-311+G (2d,2p)|SDD basis set was adopted in single point energy calculations done by using M062x and B3LYP-D3 on the M062x optimized geometries. In the potential energy surfaces (PESs), the reported energies include the ZPE corrections, excluding the contributions of frozen atoms in vibrational analysis[34] and the standard approximation for free energy. In order to properly take into account the entropic contributions, free energy corrections have been estimated adding a term equal to RT ln ($V_{\text{molar gas}}/V_{\text{molar solution}}$), where R = gas constant, T = absolute temperature, $V_{\text{molar gas}}$ is the volume occupied by one mole of ideal gas at the considered temperature and $V_{\text{molar solution}}$ is the volume occupied by one mole of species in a standard solution of concentration 1 mol L^{-1}, as successfully adopted in other works.[35,36] To obtain internal entropies, we interpolate the rotational and harmonic vibrational approximations. S_V and S_R are combined by using a weighting function, following the Head-Gordon damping function, reported in eqn (1) and (2) as proposed by S. Grimme.[18]

$$S = W(\omega)S_V + [1 - W(\omega)]S_R \quad (1)$$

$$W(\omega) = 1[1 + (\omega_0/\omega)^a]^{-1} \quad (2)$$

NBO[37] analysis was performed on all the stationary points intercepted on the PESs and the related results are given in Table S1.†

Results and discussion

Active site model

The starting molecular model used for the QM calculations was obtained from the X-ray structure of the adduct formed in the reaction between pancreatic ribonuclease isolated from *Bos taurus*[10] and arsenoplatin-1 at a resolution of 2.15 Å (PDB id: 5NJ7). All protonation states were obtained using Propka 3.0 (see Table S2†).[38,39]

To construct the active site model in the initial enzyme–substrate complex form, the Nδ (His119)–Pt was broken and modified back to the native form with the H_2O molecule replacing the imidazole ring of the His119 residue. The resulting cluster (depicted in Fig. 1) consists of 255 atoms with an overall charge of zero and contains amino acid residues of the active site positioned in the solvent exposed surface of the protein of the catalytic groove, which are Lys1, Glu2, Lys 7, Phe8, Glu9, Arg10, Gln11, His12, Val118, Phe120, and Asp121. RNase A shows a V-shaped kidney structure, with two opposite domains forming an elongated substrate-binding groove between the two arms. The high content of positively charged (lysine and arginine) residues present in the active site cleft is linked to the reaction catalyzed by RNase A consisting of the hydrolysis of the phosphodiesteric bond at the 5′-ribose of the negatively charged substrate, single-stranded RNA.

Other polar residues ensure a dense network of local interactions. The distribution of the positively and negatively charged polar and nonpolar residues is shown in Fig. 2a, where it is possible to see that His119, present along the walls of the active site groove, is surrounded almost exclusively by polar residues. The dominant distribution of these polar amino acids at the protein surface attracts water molecules in the first hydration shell. A detailed analysis of the water molecule distribution in the binding cavity in the RNase A protein has been done by using Molecular Dynamics simulations (see the ESI†). The H-bonding interactions from the MD simulation of the apoprotein are also reported in Table S3.† Fig. 2b shows the water radial distribution function (RDF) obtained as a function of the distance between the water oxygen and the Nδ of the His119 residue. The observed trend of RDF, evidenced by the sharp peak circled in orange at a distance of <2.50 Å, indicates that a more ordered water structure is present in the proximity of the protein surface rather than in bulk water where broader peaks are present. This behavior is essentially due to the specific interactions between His119 and water.

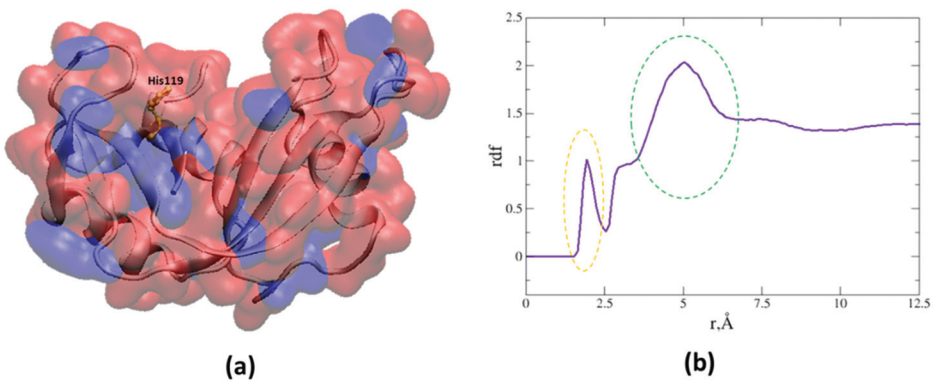

Fig. 2 (a) Structure of RNase A with the backbone evidencing the secondary structures. The surface is illustrated based on the different nature (negative, red and positive, blue) of the residues. (b) The radial distribution function of the bulk water inside 12.5 Å from Nδ of the His119 residue.

This confirms the presence of a conspicuous number of water molecules in the crystal that encouraged us to retain two explicit water molecules (**W1** and **W2**) in the QM cluster (Fig. 1).

Small models

Preliminary calculations were carried out on small models (single amino acids and platinum complex), as depicted in Scheme S1,† in order to evaluate the reactivity of **AP1** in its original form with the chloride ligand (a) or in its corresponding aquated form (b) towards histidine and methionine. The barriers related to the platination process on the small models are reported in Fig. S1.† The results confirmed that the more favorable energetics concern the aquated form of **AP1** ((b) of Scheme S1†) and the histidine resulted in the preferred target in agreement with the experimental observations.[10]

This behavior is similar to that occurring in platinum ligation to DNA purine bases investigated previously.[6] Furthermore, the energy trend obtained using the two functionals (Fig. S1†) is similar and matches well with a recent study performed on analog platinum(II) complexes.[40]

Reaction mechanism

From the water exposure of the binding pocket of RNase A and the results from our calculations on small models (see Fig. S1†), we believed that the ligation to histidine of the RNase A takes place by the aquated form **APw** and not by **AP1** (Scheme 1).

The explored mechanism for the platination of RNase A (studied by employing the larger cluster), shown in Scheme 2, indicated as **E**, proposes a single step process in which, after the barrierless formation of the adduct (**EAPw**), the reaction proceeds towards the covalent product (**P**) through a transition state characterized by the Pt of **APw** linked to Nδ of His119 and the water molecule.

All the M062x/6-31+G(d)|SDD optimized structures for the obtained stationary points are depicted in Fig. 3 along with the main geometrical parameters, while Fig. 4 shows the M062x-D3 (a) and B3LYP-D3 (b) potential energy surfaces in protein and water environments.

In the **EAPw** complex (see Fig. 3), **APw** is found to bind such that the water coordinated to Pt points toward the Nδ of His119 establishing a H-bond of 1.55 Å. An additional H-bond interaction involves the O_3H moiety and the carbonyl group of the backbone of the Phe120 residue (1.61 Å). The distance between Nδ His119 and Pt, corresponding to the reaction coordinate linking the starting point to the product of the platination process, is equal to 3.83 Å. This confirms that the neutral nucleophile His119 is not still included in the inner coordination shell of the platinum, thus ensuring the planarity around the Pt center since the dihedral angle (N2–N1–O1–O2) is −3.54°. The **EAPw** complex is 4.30 (3.83) kcal mol^{-1} at M062x-D3 (B3LYP-D3) lower than the separated reactants (**E** + **APw**) in the protein environment and the corresponding values in the water phase are 0.90 kcal mol^{-1} (M062x-D3) and 2.37 kcal mol^{-1} (B3LYP-D3) (Fig. 3).

The reaction proceeds towards the product by overcoming the barrier dictated by the **TS** whose optimized structure is depicted in Fig. 3. The RNase A platination process takes place at the expense of His119 (Nδ imidazole ring) that now is located at 2.83 Å, confirming the shortening of the distance by 1 Å with respect to the **EAPw** adduct. The water molecule is placed at 2.16 Å showing only slight lengthening relative to the previous species. This behaviour can be assimilated to an associative-like substitution mechanism in which the incoming ligand (His119) binds to the Pt center before the departing ligand (water). The Pt appears pentacoordinated and arranged in a trigonal bipyramidal geometry as also observed in the corresponding step of the **AP1** aquation process.[6] The imaginary frequency in this **TS** is about 59 cm^{-1} and the analysis of

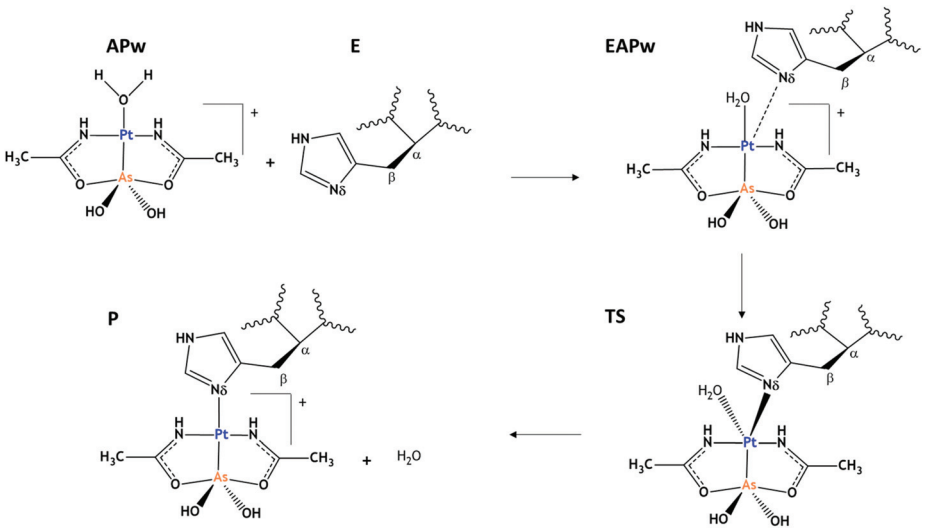

Scheme 2 The mechanism of the metalation process promoted by **APw**.

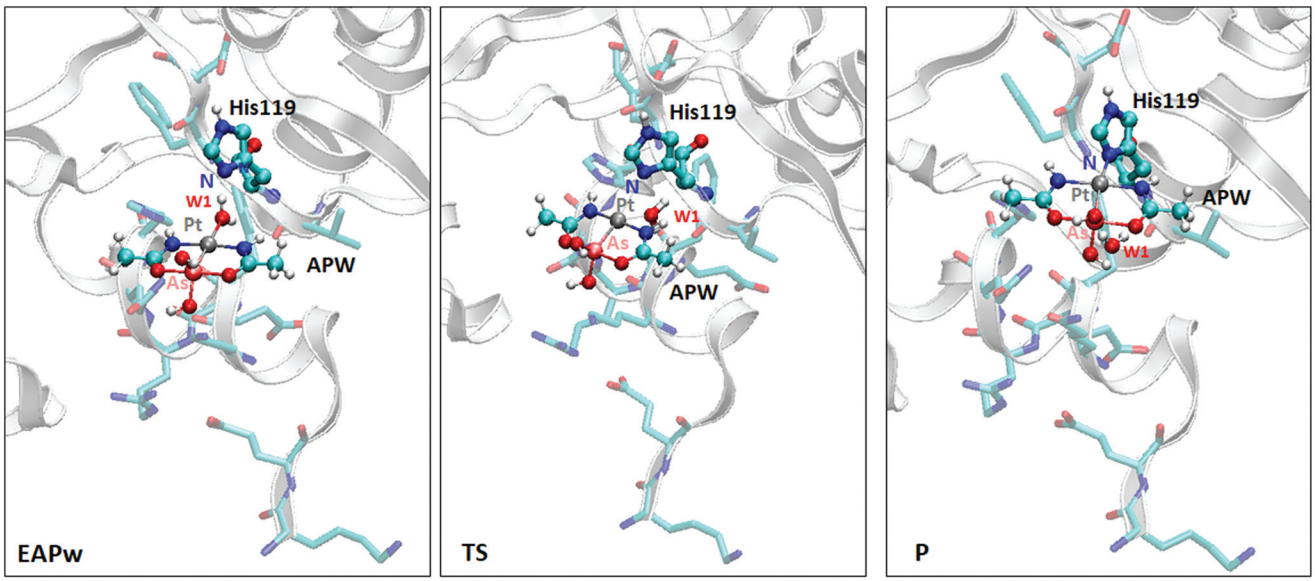

Distance (Å)	EAPw	TS	P	X-Ray[a]
Pt-N_{His}	3.83	2.83	2.21	2.10
Pt-As	2.30	2.32	2.32	2.20
Pt-Ow	2.16	2.30	3.37	4.02
Pt-N1	2.03	2.03	2.03	2.00
Pt-N2	2.04	2.04	2.07	2.00
As-O1	1.94	1.96	1.96	1.98
As-O2	1.99	1.99	1.97	2.02
As-O3	1.73	1.74	1.74	1.72
As-O4	1.74	1.72	1.73	1.72
H_w-N_{his}	1.55	1.75	2.23	4.25
Angle (°)				
N-Pt-O	43.78	61.97	62.69	84.40

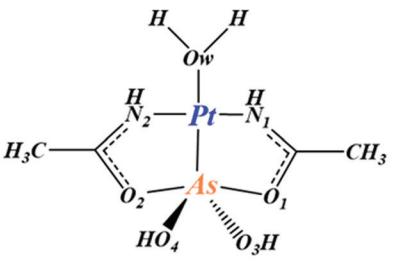

Fig. 3 Optimized geometries of the stationary points at the M062x/6-31G+(d,p)|SDD level of theory. [a] Main distances as defined in the structure are included in the connected table.[10]

the corresponding vibrational mode clearly indicates the stretching of the Nδ His119–Pt bond formation associated with that of metal–water (Pt–Ow).

The required energetic cost for this step is about 15 kcal mol^{-1} using both M062x-D3 and B3LYP-D3 functionals in the protein environment. The same barrier is reduced to about 9 and 10 kcal mol^{-1} in water (see Fig. 4). This can be considered the consequence of the "synergic" effect due to the destabilization of the **EAPw** adduct and the stabilization of the transition state observed with both the employed functionals. This evidence further highlights the role played by the first hydration shell of the protein surface around the Pt where the bond cleavage and formation occur.

As evidenced above in the small models, in the QM cluster larger model, both the used functionals provide electronic barrier heights and electronic energies very close in energy in the protein and water environments as in the case of other chemical reactions.[41] Furthermore, the inclusion of D3 dispersion does not influence the energetics of the process.

Looking at the NBO charges collected in Table S1,† it is possible to note that the charge on Pt in the **TS** becomes less positive than that in the adduct due to the effect of the presence of different atoms of the ligand (Ow in **EAPw** and Nδ in the **TS**) on the metal center. In the final platinated complex (**P**) the imidazole of His119 lies in the trans position to the As $(OH)_2$ moiety at about 2.21 Å from Pt while the water leaving group is now at 3.37 Å and is in close contact with His119 by an H-bond (2.23 Å). During the platination process the geometrical parameters in the $As(OH)_2$ and diacetylamido moieties do not suffer significant variations and the Pt–As bond maintains the same distance (see Fig. 2). This behavior is in agreement with that of the experimental counterpart that proposes the Pt–As unit to remain intact upon RNase A binding. The additional water molecule (**W2**) retained in the QM model lies very close to the platination reaction site establishing an H-bond (2.00 Å) interaction with the oxygen atom of the Val118 residue, and with the backbone N atom of Phe8 with an N–Hw distance of 2.30 Å.

The stability of the final covalent platinated product with the Nδ–Pt formed bond is confirmed by the ΔG value of the process that is a little bit more pronounced with B3LYP-D3 than that with M062x-D3 (see Fig. 4). The exothermicity of the

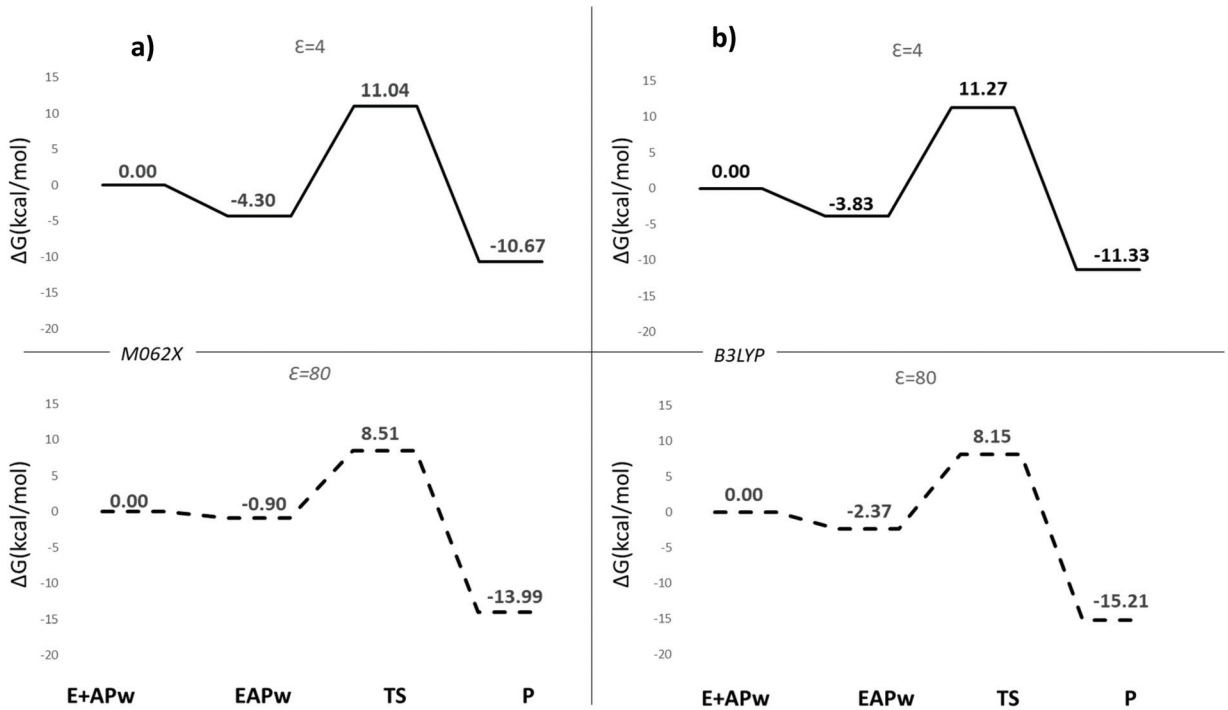

Fig. 4 M062x-D3/6-311+G(2d,2p)|SDD//M062x/6-31+G(d,p)|SDD (a) and B3LYP-D3/6-311+G(2d,2p)|SDD//M062x/6-31+G(d,p)|SDD (b) free energy profiles of the RNase A metalation process promoted by **APw** in protein (ε = 4) and water (ε = 80) environments.

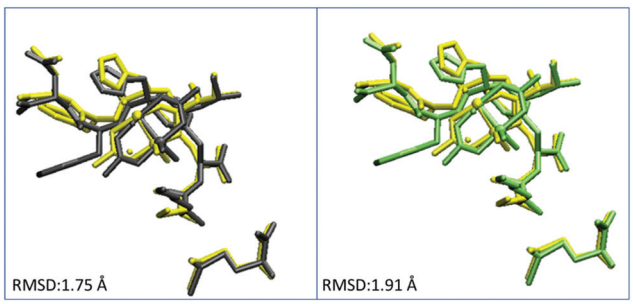

Fig. 5 Superposition of the M062x/6-31+G(d)|SDD (gray) and B3LYP-D3/6-31+G(d)|SDD (green) optimized structures of the final covalent platinated product (**P**) with the corresponding crystallographic structure (yellow).

process indicates that the reverse reaction is still possible but much slower for the higher barriers (21.71 and 22.50 kcal mol^{-1} at the M062x level and 22.60 and 23.36 kcal mol^{-1} at the B3LYP-D3 level in protein and water environments, respectively).

Comparison with the experimental results,[10] (see Fig. 5) possible only for the **P** species, shows a good agreement with the calculated geometry with both the employed functionals as indicated by the superposition of the optimized structure of **P**.

To better evaluate the nature of the interactions present inside the catalytic pocket during the process, in Fig. 6, we have reported the density of isosurfaces, arising from Non-Covalent Interactions (NCI) analysis, indicating the contributions of the residues retained in the model. The red isosur-

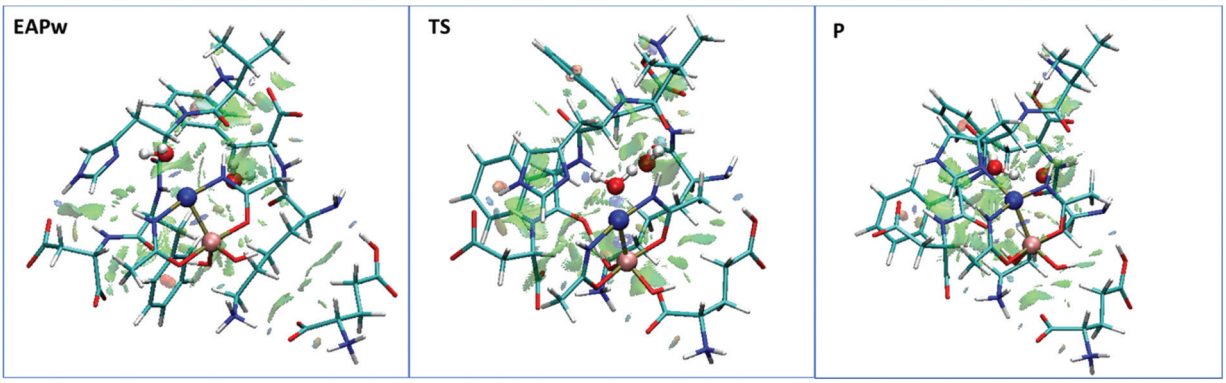

Fig. 6 Nonbonding interaction plot calculated for the stationary points at the M062x/6-311+G(2d,2p)|SDD//M062x/6-31+G(d,p)|SDD level.

faces account for the repulsive interactions related to the center of the π systems of Phe8 and Phe120 residues. Further information arises from the green regions indicative of the dispersion contributions (van der Waals forces) characterizing the binding cavity of the adduct that increases during the platination process (**EAPw** → **P**). The blue region around Pt reveals significant attractive interactions (H-bond) that are absent in the **EAPw** but appear in the **TS** structure where **W1** engages Nδ of His119 and the **W2** molecule forms a H-bond.

Conclusions

Drug discovery remains a great challenge for scientific and economic reasons. In particular, the development of new anticancer agents is a long-term process, which involves multiple steps and can not always exclude the occurrence of side effects. The preparation of hybrid molecules with two or more structural domains acting as two distinct pharmacophores represents a more fast and efficient pathway. This is particularly the case of arsenoplatin-1 (**AP1**), $[Pt(\mu\text{-}NHC(CH_3)O)_2ClAs(OH)_2]$, the object of the theoretical investigation presented herein. It is a new anticancer agent that is more active than the parent drugs As_2O_3 and cisplatin in most of the cancer cell lines tested. The metalation process of RNase A by **AP1** has been elucidated by DFT calculations using a larger cluster model able to represent the environment of the binding site of **AP1** quite realistically. The proposed one-step mechanism of the RNase A inhibition by **AP1**, examined in both protein and water environments by the solvation continuum model, shows low barriers compatible with a very fast process. The occurrence in aqueous medium is more favorable from a kinetic point of view with both B3LYP and M062x functionals and compatible with the protein's active site present on the surface area accessible to solvents. The structure of the metalated protein product (**P**) matches very well with the corresponding crystallographic one, confirming that the binding site is well reproduced by the used cluster model.

Conflicts of interest

The authors declare that the research was conducted in the absence of any potential conflict of interest.

Acknowledgements

The Università degli Studi della Calabria-Dipartimento di Chimica e Tecnologie Chimiche (CTC) is gratefully acknowledged.

References

1 H. Chen, S. Pazicni, N. Krett, R. Ahn, J. Penner-Hahn, S. Rosen and T. O'Halloran, Coencapsulation of Arsenic- and Platinum-Based Drugs for Targeted Cancer Treatment, *Angew. Chem.*, 2009, **121**, 9459–9463.

2 Đ. U. Miodragović, J. A. Quentzel, J. W. Kurutz, C. L. Stern, R. W. Ahn, I. Kandela, A. Mazar and T. V. O'Halloran, Robust Structure and Reactivity of Aqueous Arsenous Acid-Platinum(II) Anticancer Complexes, *Angew. Chem., Int. Ed.*, 2013, **52**, 10749–10752.

3 C. Zheng, S. Lam, Y. Li, B. M. Fong, J. C. Mak and J. C. Ho, Combination of Arsenic Trioxide and Chemotherapy in Small Cell Lung Cancer, *Lung Cancer*, 2013, **82**, 222–230.

4 T. Nakaoka, A. Ota, T. Ono, S. Karnan, H. Konishi, A. Furuhashi, Y. Ohmura, Y. Yamada, Y. Hosokawa and Y. Kazaoka, Combined Arsenic Trioxide-Cisplatin Treatment Enhances Apoptosis in Oral Squamous Cell Carcinoma Cells, *Cell. Oncol.*, 2014, **37**, 119–129.

5 N. Zhang, Z.-M. Wu, E. McGowan, J. Shi, Z.-B. Hong, C.-W. Ding, P. Xia and W. Di, Arsenic Trioxide and Cisplatin Synergism Increase Cytotoxicity in Human Ovarian Cancer Cells: Therapeutic Potential for Ovarian Cancer, *Cancer Sci.*, 2009, **100**, 2459–2464.

6 T. Marino, A. Parise and N. Russo, The Role of Arsenic in the Hydrolysis and DNA Metalation Processes in an Arsenous Acid–Platinum(II) Anticancer Complex, *Phys. Chem. Chem. Phys.*, 2017, **19**, 1328–1334.

7 A. Merlino, T. Marzo and L. Messori, Protein Metalation by Anticancer Metallodrugs: A Joint ESI MS and XRD Investigative Strategy, *Chem. – Eur. J.*, 2017, **23**, 6942–6947.

8 L. Messori and A. Merlino, Protein Metalation by Metal-Based Drugs: X-Ray Crystallography and Mass Spectrometry Studies, *Chem. Commun.*, 2017, **53**, 11622–11633.

9 A. Casini, G. Mastrobuoni, C. Temperini, C. Gabbiani, S. Francese, G. Moneti, C. T. Supuran, A. Scozzafava and L. Messori, ESI Mass Spectrometry and X-Ray Diffraction Studies of Adducts between Anticancer Platinum Drugs and Hen Egg White Lysozyme, *Chem. Commun.*, 2007, 156–158.

10 Đ. Miodragović, A. Merlino, E. P. Swindell, A. Bogachkov, R. W. Ahn, S. Abuhadba, G. Ferraro, T. Marzo, A. P. Mazar, L. Messori and T. V. O'Halloran, Arsenoplatin-1 Is a Dual Pharmacophore Anticancer Agent, *J. Am. Chem. Soc.*, 2019, **141**, 6453–6457.

11 M. Frisch, G. Trucks, H. Schlegel, G. Scuseria, M. Robb, J. Cheeseman, G. Scalmani, V. Barone, B. Mennucci, G. Petersson, H. Nakatsuji, M. Caricato, X. Li, H. Hratchian, A. Izmaylov, J. Bloino, G. Zheng, J. Sonnenberg, M. Hada, M. Ehara, K. Toyota, R. Fukuda, J. Hasegawa, M. Ishida, T. Nakajima, Y. Honda, O. Kitao, H. Nakai, T. Vreven, J. Montgomery, J. Peralta, F. Ogliaro, M. Bearpark, J. Heyd, E. Brothers, K. Kudin, V. Staroverov, R. Kobayashi, J. Normand, K. Raghavachari, A. Rendell, J. Burant, S. Iyengar, J. Tomasi, M. Cossi, N. Rega, J. Millam, M. Klene, J. Knox, J. Cross, V. Bakken, C. Adamo, J. Jaramillo, R. Gomperts, R. Stratmann, O. Yazyev, A. Austin, R. Cammi, C. Pomelli, J. Ochterski, R. Martin, K. Morokuma, V. Zakrzewski, G. Voth, P. Salvador, J. Dannenberg, S. Dapprich, A. Daniels, Ö. Farkas,

J. Foresman, J. Ortiz, J. Cioslowski and D. Fox, *Gaussian 09, Revision D.01*, Gaussian, Inc., Wallingford CT.

12 A. D. Becke, Density–functional Thermochemistry. III. The Role of Exact Exchange, *J. Chem. Phys.*, 1993, **98**, 5648–5652.

13 C. Lee, W. Yang and R. G. Parr, Development of the Colle-Salvetti Correlation-Energy Formula into a Functional of the Electron Density, *Phys. Rev. B: Condens. Matter Mater. Phys.*, 1988, **37**, 785–789.

14 Y. Zhao and D. G. Truhlar, The M06 Suite of Density Functionals for Main Group Thermochemistry, Thermochemical Kinetics, Noncovalent Interactions, Excited States, and Transition Elements: Two New Functionals and Systematic Testing of Four M06-Class Functionals and 12 Other Functionals, *Theor. Chem. Acc.*, 2008, **120**, 215–241.

15 D. Andrae, U. Hausermann, M. Dolg, H. Stoll and H. Preuss, Energy-Adjustedab Initio Pseudopotentials for the Second and Third Row Transition Elements, *Theor. Chim. Acta*, 1990, **77**, 123–141.

16 S. Grimme, J. Antony, S. Ehrlich and H. Krieg, A Consistent and Accurate *Ab Initio* Parametrization of Density Functional Dispersion Correction (DFT-D) for the 94 Elements H-Pu, *J. Chem. Phys.*, 2010, **132**, 154104.

17 T. Vreven, K. S. Byun, I. Komáromi, S. Dapprich, J. A. Montgomery, K. Morokuma and M. J. Frisch, Combining Quantum Mechanics Methods with Molecular Mechanics Methods in ONIOM, *J. Chem. Theory Comput.*, 2006, **2**, 815–826.

18 S. Grimme, Supramolecular Binding Thermodynamics by Dispersion-Corrected Density Functional Theory, *Chem. – Eur. J.*, 2012, **18**, 9955–9964.

19 R. P. P. Neves, P. A. Fernandes and M. J. Ramos, Mechanistic Insights on the Reduction of Glutathione Disulfide by Protein Disulfide Isomerase, *Proc. Natl. Acad. Sci. U. S. A.*, 2017, **114**, E4724–E4733.

20 F. E. Medina, R. P. P. Neves, M. J. Ramos and P. A. Fernandes, QM/MM Study of the Reaction Mechanism of the Dehydratase Domain from Mammalian Fatty Acid Synthase, *ACS Catal.*, 2018, **8**, 10267–10278.

21 F. E. Medina, M. J. Ramos and P. A. Fernandes, Complexities of the Reaction Mechanisms of CC Double Bond Reduction in Mammalian Fatty Acid Synthase Studied with Quantum Mechanics/Molecular Mechanics Calculations, *ACS Catal.*, 2019, **9**, 11404–11412.

22 M. Prejanò, T. Marino and N. Russo, On the Inhibition Mechanism of Glutathione Transferase P1 by Piperlongumine. Insight From Theory, *Front. Chem.*, 2018, **6**, 606.

23 M. R. A. Blomberg, T. Borowski, F. Himo, R.-Z. Liao and P. E. M. Siegbahn, Quantum Chemical Studies of Mechanisms for Metalloenzymes, *Chem. Rev.*, 2014, **114**, 3601–3658.

24 A. J. M. Ribeiro, M. E. Alberto, M. J. Ramos, P. A. Fernandes and N. Russo, The Catalytic Mechanism of Protein Phosphatase 5 Established by DFT Calculations, *Chem. – Eur. J.*, 2013, **19**, 14081–14089.

25 P. Piazzetta, T. Marino and N. Russo, Insight into the Promiscuous Activity of Human Carbonic Anhydrase against the Cyanic Acid Substrate from a Combined QM and QM/MM Investigation, *Phys. Chem. Chem. Phys.*, 2014, **16**, 16671.

26 A. J. M. Ribeiro, D. Santos-Martins, N. Russo, M. J. Ramos and P. A. Fernandes, Enzymatic Flexibility and Reaction Rate: A QM/MM Study of HIV-1 Protease, *ACS Catal.*, 2015, **5**, 5617–5626.

27 H. Chen, S. Pazicni, N. Krett, R. Ahn, J. Penner-Hahn, S. Rosen and T. O'Halloran, Coencapsulation of Arsenic- and Platinum-Based Drugs for Targeted Cancer Treatment, *Angew. Chem.*, 2009, **121**, 9459–9463.

28 R.-Z. Liao, F. Himo, J.-G. Yu and R.-Z. Liu, Dipeptide Hydrolysis by the Dinuclear Zinc Enzyme Human Renal Dipeptidase: Mechanistic Insights from DFT Calculations, *J. Inorg. Biochem.*, 2010, **104**, 37–46.

29 C. Gonzalez and H. B. Schlegel, An Improved Algorithm for Reaction Path Following, *J. Chem. Phys.*, 1989, **90**, 2154–2161.

30 C. Gonzalez and H. Bernhard, Schlegel, Reaction Path Following in Mass-Weighted Internal Coordinates, *J. Phys. Chem.*, 1990, **94**, 5523–5527.

31 M. Cossi, N. Rega, G. Scalmani and V. Barone, Structures, and Electronic Properties of Molecules in Solution with the C-PCM Solvation Model, *J. Comput. Chem.*, 2003, **24**, 669–681.

32 V. Barone and M. Cossi, Quantum Calculation of Molecular Energies and Energy Gradients in Solution by a Conductor Solvent Model, *J. Phys. Chem. A*, 1998, **102**, 1995–2001.

33 J. Yan and S. Chen, How To Produce Methane Precursor in the Upper Ocean by An Untypical Non–Heme Fe–Dependent Methylphosphonate Synthase?, *ChemPhysChem*, 2020, **21**, 385–396.

34 M. Prejanò, I. Romeo, L. Sgrizzi, N. Russo and T. Marino, Why Hydroxy-Proline Improves the Catalytic Power of the Peptidoglycan *N* -Deacetylase Enzyme: Insight from Theory, *Phys. Chem. Chem. Phys.*, 2019, **21**, 23338–23345.

35 M. Prejanò, N. Russo and T. Marino, How Lanthanide Ions Affect the Addition–Elimination Step of Methanol Dehydrogenases, *Chem. – Eur. J.*, 2020, **26**, 11334–11339.

36 E. D. Glendening, A. E. Reed, J. E. Carpenter and F. Weinhold, *NBO, Version 3.1*, Theoretical Chemistry Institute, University of Wisconsin, Madison, 1995.

37 P. E. M. Siegbahn and F. Himo, Recent Developments of the Quantum Chemical Cluster Approach for Modeling Enzyme Reactions, *JBIC, J. Biol. Inorg. Chem.*, 2009, **14**, 643–651.

38 V. Srivastava, In Situ Generation of Ru Nanoparticles to Catalyze CO_2 Hydrogenation to Formic Acid, *Catal. Lett.*, 2014, **144**, 1745–1750.

39 F. J. Pérez-Alonso, M. L. Granados, M. Ojeda, T. Herranz, S. Rojas, P. Terreros, J. L. G. Fierro, M. Gracia and J. R. Gancedo, Relevance in the Fischer–Tropsch Synthesis of the Formation of Fe–O–Ce Interactions on Iron–Cerium

Mixed Oxide Systems, *J. Phys. Chem. B*, 2006, **110**, 23870–23880.

40 I. Tolbatov, C. Coletti, A. Marrone and N. Re, Reactivity of arsenoplatin complex versus water and thiocyanate: a DFT benchmark study, *Theor. Chem. Acc.*, 2020, **139**, 184.

41 A. T. Pereira, A. J. M. Ribeiro, P. A. Fernandes and M. J. Ramos, Benchmarking of density functionals for the kinetics and thermodynamics of the hydrolysis of glycosidic bonds catalyzed by glycosidases, *Int. J. Quantum Chem.*, 2017, **117**, e25409.